Estimation of Regional Evapotranspiration by TM/ETM+ Data over Heterogeneous Surfaces

Shaomin Liu, Guang Hu, Li Lu, and Defa Mao

Abstract

Evapotranspiration is an important part in surface energy balance and water balance. Compared with other methods (micrometeorological, climatological, or hydrological method), the remote sensing model has obvious superiority to estimate regional evapotranspiration over heterogeneous surfaces. In this study, based on Landsat TM/ETM+ data and meteorological data, evapotranspiration in Beijing area on 17 April 2001, 12 April 2002, 06 July 2004, 06 May 2005, and 22 May 2005 were calculated by an estimation model of regional evapotranspiration. Comparisons of energy balance components (net radiation, soil heat flux, sensible and latent heat flux) with measured fluxes were made integrating the remotely sensed fluxes by the footprint model. Results show that latent heat flux estimates (adjusted for closure) with errors (MBE±RMSE) 26.47±42.54 Wm^{-2}, sensible heat flux error of −8.56±23.79 Wm^{-2}, net radiation error of 25.16±50.87 Wm^{-2} and soil heat flux error of 10.68±22.81 Wm^{-2}. The better agreement between the estimates and the measurements indicates that the remote sensing model is appropriate for estimating regional evapotranspiration over heterogeneous surfaces. Furthermore, the spatial distribution of evapotranspiration in Beijing area was analyzed.

Introduction

Evapotranspiration (ET) plays an important role in energy exchange and hydrological cycle between the land surface and atmosphere. Estimating ET accurately is a key point in many fields such as geography, meteorology, hydrology, and ecology. Along with the development of remote sensing technology, the estimation models of regional ET with remote sensing data have been mainly developed in last two decades, bringing us a hope to estimate regional ET over heterogeneous surfaces. Generally, the estimation models of regional ET with remote sensing data can be divided into two main categories: (a) to estimate ET by means of an index (e.g., the Crop Water Stress Index, Surface Energy Balance Index) using a combination equation (Jackson *et al.*, 1981; Menenti and Choudhury, 1993; Moran *et al.*, 1994 and 1996), and (b) to calculate the net radiation, soil heat flux, and sensible heat flux first and then to obtained ET as the residual in the energy balance equation. This kind of model includes the single source model (Jackson, 1985; Choudhury *et al.*, 1986; Kustas *et al.*, 1989; Bastiaanssen *et al.*, 1998; Su, 2002) and the double source model (Shuttleworth and Wallace, 1985; Norman *et al.*, 1995; Blyth *et al.*, 1995), on the basis of different land surface descriptions. Among the two kinds of estimation models of regional ET, the energy balance model is now the most popular method.

In this study, an estimation model of regional ET with Landsat TM/ETM+ data was proposed and applied to a case study of Beijing. The remote sensing estimates were compared with measured fluxes. Footprint weights were used to integrate remotely sensed fluxes.

Methodology

The estimation model of regional ET with TM/ETM+ data has many sub-models and can be seen in Figure 1.

The ET is calculated as the residual in the surface energy balance equation:

$$LE = R_n - G - H \tag{1}$$

where LE is the latent heat flux (ET expressed in energy units); L is the latent heat of vaporization; R_n is the net radiation; G is the soil heat flux; and H is the sensible heat flux.

Net Radiation

Net radiation R_n is calculated as:

$$R_n = (1 - \alpha)Q + \varepsilon\varepsilon_a\sigma T_a^4 - \varepsilon\sigma T_s^4 \tag{2}$$

where Q is the global short-wave radiation, which is a function of the solar constant, the atmospheric transmittance, the sun-earth distance correction factor and the solar zenith angle; σ is the Stefan-Boltzman constant; T_a is the air temperature; and α is the surface broadband albedo and is estimated by TM/ETM+ spectral albedo (Liang, 2001):

$$\alpha = 0.356\alpha_1 + 0.13\alpha_3 + 0.373\alpha_4 + 0.085\alpha_5 + 0.072\alpha_7 \tag{3}$$

where α_1, α_3, α_4, α_5, and α_7 are the spectral albedo of the first, third, forth, fifth, and seventh channel in TM/ETM+, respectively. ε_a is the atmospheric emissivity, according to Brutsaert (1975):

$$\varepsilon_a = 9.2 \times 10^{-6} \times T_a^2. \tag{4}$$

Surface emissivity ε is expressed as (Valor and Casellers, 1996):

$$\varepsilon = \varepsilon_v \cdot f + \varepsilon_g \cdot (1 - f) + d\varepsilon \tag{5}$$

Shaomin Liu, Guang Hu, and Li Lu are with the State Key Laboratory of Remote Sensing Science, School of Geography, Beijing Normal University, No.19, Xinjiekouwai Street, Beijing 100875, China (smliu@bnu.edu.cn).

Defa Mao is with the Beijing Water Technology Center, Beijing 100073, China.

Photogrammetric Engineering & Remote Sensing
Vol. 73, No. 10, October 2007, pp. 1169–1178.

0099-1112/07/7310–1169/$3.00/0

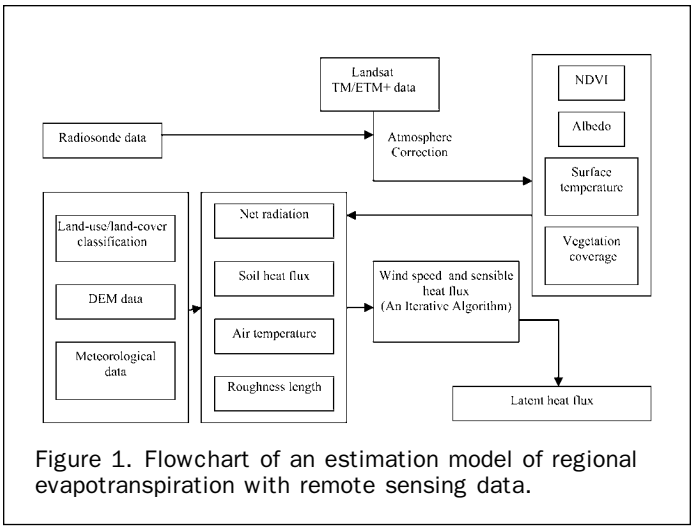

Figure 1. Flowchart of an estimation model of regional evapotranspiration with remote sensing data.

where two surface emissivities are used in this study. The first is an emissivity representing surface behavior for thermal emission in the relatively narrow band 6 of Landsat (10.4 to 12.5 μm). The second is used to calculate the longwave radiation emission from the surface (8 to 14 μm). The emissivity of vegetation, ε_v, is taken as 0.985 (0.985) (the one in parentheses is the second emissivity). The emissivity ε_g is taken as 0.97(0.962), 0.99 (0.985), and 0.96(0.95) for bare soil, water, urban and road, respectively (Sobrino *et al.*, 2004; Hu, 2006). $d\varepsilon$ is a regional representative value accounting for multiple scattering and is neglected here. f is the fractional vegetation cover (Gutman and Ignatov,1998):

$$f = \frac{NDVI - NDVI_{\min}}{NDVI_{\max} - NDVI_{\min}} \tag{6}$$

where $NDVI_{\min}$ and $NDVI_{\max}$ are the minimum and maximum NDVI in the study area.

Surface temperature T_s is retrieved by the mono-window algorithm (Qin *et al.*, 2001):

$$T_s = \frac{a(1 - c - d) + [b(1 - c - d) + c + d]T_{sensor} - cT_0}{c} \tag{7}$$

where $a = -67.35535$, $b = 0.458608$, $c = \varepsilon\tau$, $d = (1 - \tau)[1 + (1 - \varepsilon)\tau]$. τ is the atmospheric transmittance and is obtained by MODTRAN with air sounding data of Beijing at 0800 time. T_{sensor} is the at-sensor brightness temperature. T_0 is the mean atmosphere temperature, according to Sobrino *et al.*, (2004):

$$T_0 = 16.0110 + 0.92621T_a. \tag{8}$$

Soil Heat Flux

For vegetated field, the soil heat flux G can be obtained following Bastiaanssen (2000):

$$G/R_n = T_s/\alpha(0.0038\alpha + 0.0074\alpha^2)(1 - 0.98NDVI^4). \tag{9}$$

For water, bare soil, and urban and road surfaces, the ratio of soil heat flux to net radiation is set to 0.5, 0.3, and 0.4-1, respectively (Waters *et al.*, 2002; Soushi, 2005).

Sensible Heat Flux

Based on the Monin-Obukhov similarity theory, the sensible heat flux H can be obtained by solving Equations 10 through 13 using an iterative algorithm:

$$H = \rho C_p \frac{(\theta_0 - \theta_a)}{r_a} \tag{10}$$

$$r_a = \frac{1}{k^2 u}\left[\ln\left(\frac{z-d}{z_{0m}}\right) - \psi_m\left(\frac{z-d}{L}\right)\right]\left[\ln\left(\frac{z-d}{z_{0h}}\right) - \psi_h\left(\frac{z-d}{L}\right)\right] \tag{11}$$

$$L = \frac{\rho \cdot C_p \cdot \boldsymbol{u}_*^3 \cdot \boldsymbol{\theta}_v}{k \cdot g \cdot H} \tag{12}$$

$$u_* = \frac{ku}{\left[\ln\left(\frac{z-d}{z_{0m}}\right) - \psi_m\left(\frac{z-d}{L}\right)\right]} \tag{13}$$

where r_a is the aerodynamic resistance, L is the Obukhov length; u_* is the friction velocity; z is the reference height; u is the wind speed; g is the acceleration of gravity; θ_0 is the potential temperature at the surface; θ_a is the potential temperature at reference height level; θ_v is the virtual potential temperature near the surface; ρ is the air density; C_p is the specific heat of air at constant pressure; k is the von Karman constant (0.4); and z_{0m} is the roughness length for momentum exchange. For vegetated field, the following empirical formula is used to estimate regional z_{0m} (Waters *et al.*, 2002):

$$z_{0m} = \exp(a\frac{NDVI}{\alpha} - b) \tag{14}$$

where a and b are empirical coefficients. In this paper, $a = 0.0553$, and $b = 3.64$ ($r^2 = 0.97$) derived by regression of observations. For forest, water, bare soil, urban and road surfaces, z_{0m} is taken as 0.5m, 0.0003m, 0.001m, and approximately 0.1 to 1.5 m, respectively (Soushi, 2005; Gao and Bian, 2002).

The roughness length for heat transfer z_{0h} in terms of kB^{-1} ($=\ln\frac{z_{0m}}{z_{0h}}$) is calculated by different parameterizations over various surfaces. For vegetated field, kB^{-1} is expressed as (Su, 2002):

$$kB^{-1} = \frac{kC_d}{4C_t\frac{u_*}{u}(1 - e^{-n/2})}f^2 + \frac{k\frac{u_*}{u}\frac{z_{0m}}{h}}{C_t^*}f^2(1-f)^2 + kB_s^{-1}(1-f)^2 \tag{15}$$

where C_d is the drag coefficient of the foliage taken as 0.2. C_t and C_t^* are heat transfer coefficient for leaf and soil surface, respectively; n is wind speed profile extinction coefficient within the canopy; h is the canopy height; kB_s^{-1} is the value for bare soil, given by $kB_s^{-1} = 2.46(\mathrm{Re}_*)^{1/4} - \ln(7.4)$, where Re_* is the roughness Reynolds number (Brutsaert, 1982).

For water and urban area, z_{0h} can be parameterized by following two equations, respectively (Brutsaert, 1982):

$$z_{0h,\ water} = 0.169\exp(-1.53u_*^{0.25}) \tag{16}$$

$$z_{0h,\ urban} = 7.4\exp(-2.46\mathrm{Re}_*^{0.25}) \times z_{0m}. \tag{17}$$

d is the zero plane displacement height and can be estimated with z_{0m} (Brutsaert, 1982):

$$d = 4.9 \times z_{0m}. \tag{18}$$

ψ_h, ψ_m are the integral form of the stability correction functions for heat transfer and momentum exchange, respectively. In unstable conditions, ψ_h, ψ_m can be expressed as (Webb, 1970; Businger *et al.*, 1971):

$$\psi_m = 2\ln\left[\frac{(1+x)}{2}\right] + \ln\left[\frac{(1+x^2)}{2}\right] - 2\arctan(x) + \frac{\pi}{2} \tag{19}$$

$$\psi_h = 2\ln\left[\frac{(1+x^2)}{2}\right]. \tag{20}$$

In stable conditions (Paulson, 1970):

$$\psi_m = \psi_h = -5\xi \tag{21}$$

where

$$\xi = (z-d)/L \tag{22}$$

$$x = (1-16\xi)^{1/4}. \tag{23}$$

Over an extremely dry surface, the evapotranspiration becomes zero due to the limitation of soil moisture. The available energy is completely converted to sensible heat flux. From Equation 1, it follows:

$$H_{dry} = R_n - G. \tag{24}$$

Over extremely wet surface, the evapotranspiration takes its potential value, the sensible heat flux is at its minimum value (Su, 2002):

$$H_{wet} = \left(R_n - G - \frac{\rho C_p}{r_{ew}}\frac{e_s - e_d}{\gamma}\right) \Big/ (1+\Delta/\gamma) \tag{25}$$

where e_s is the saturated vapor pressure; e_d is the actual vapor pressure; Δ is the slope of saturated vapor pressure with air temperature; γ is the psychrometer constant; and r_{ew} is the aerodynamic resistance over wet surface.

In this study, when $H > H_{dry}$, then $H = H_{dry}$; when $H < H_{wet}$, then $H = H_{wet}$.

Study Area and Data

Study Area

Beijing area (39°25′12″N, 41°3′36″N; 115°24′36″E, 117°31′12″E) is located in the northern part of the North China Plain, with the Loess Plateau to its west and Inner Mongolian Plateau to its north. The area average (1961 to 1990) annual temperature is 11.8°C, with January and July temperature of −3.9°C and 26.2°C, respectively, and the annual precipitation is 576.9 mm.

Beijing has twelve districts and six counties. A map of the area, including the location of its 19 meteorological stations, can be seen in Figure 2. The land-use/land-cover types are shown in Figure 3.

Remote Sensing and Meteorological Data

The five TM/ETM+ images used in this study are 17 April 2001, 12 April 2002, 06 July 2004, 06 May 2005, and 22 May 2005 over Beijing area. The DEM at the scale of 1:50 000 (Figure 4), as well as the maps of land-use/land-cover classifications (1:100 000) and administrative divisions (1:100 000) are also collected.

Figure 2. Administrative divisions and meteorological stations distribution in Beijing.

Meteorological data consist of air temperature, wind, and aerological soundings collected at the 19 meteorological stations of China Meteorological Administration. The observations are only three to four times per day, and do not match with the time of satellite overpass. The spatial gridded data at overpass time are made through temporal and spatial interpolation. Air temperature at the time of satellite overpass can be obtained by a harmonic method, assuming that the diurnal air temperature is adequately described by a sine function at every meteorological station (Tu *et al.*, 1978). To obtain air temperature at the pixel scale, the data are first converted to corresponding sea-level values according to the altitude of the meteorological stations, and then interpolated using the Kriging method. With DEM data, the sea-level air temperature images are further converted to the actual air temperature by assuming a lapse rate of 0.5°C per 100 m (Weng and Sun, 1984).

In this study, a linear method is used for temporal interpolation of wind speed. A method based on surface roughness length is proposed for spatial interpolation of wind speed (Zhang *et al.*, 2003):

$$\frac{u_{-p}}{u_{-s}} = \frac{\ln\left(\frac{z-d_{-p}}{z_{0m-p}}\right) - \psi_{m-p}}{\ln\left(\frac{z-d_{-s}}{z_{0m-s}}\right) - \psi_{m-s}} \tag{26}$$

where u_{-s}, z_{0m-s}, d_{-s}, and ψ_{m-s} are wind speed, the roughness length for momentum exchange, zero plane displacement height, and the stability correction function for momentum exchange at the nearby meteorological station, respectively; u_{-p}, z_{0m-p}, d_{-p}, and ψ_{m-p} are the respective value at each pixel. During processing, at first, wind speed of the nearby meteorological station is used in Equations 10 through 13 to obtain H and L of the pixel where the meteorological station is located. Then, the stability correction function for momentum exchange at the nearby meteorological station ψ_{m-s} is calculated with Equations 19 and 21. Last, wind speed of the pixel is obtained by solving the set of Equations 10 through 13 and Equation 26.

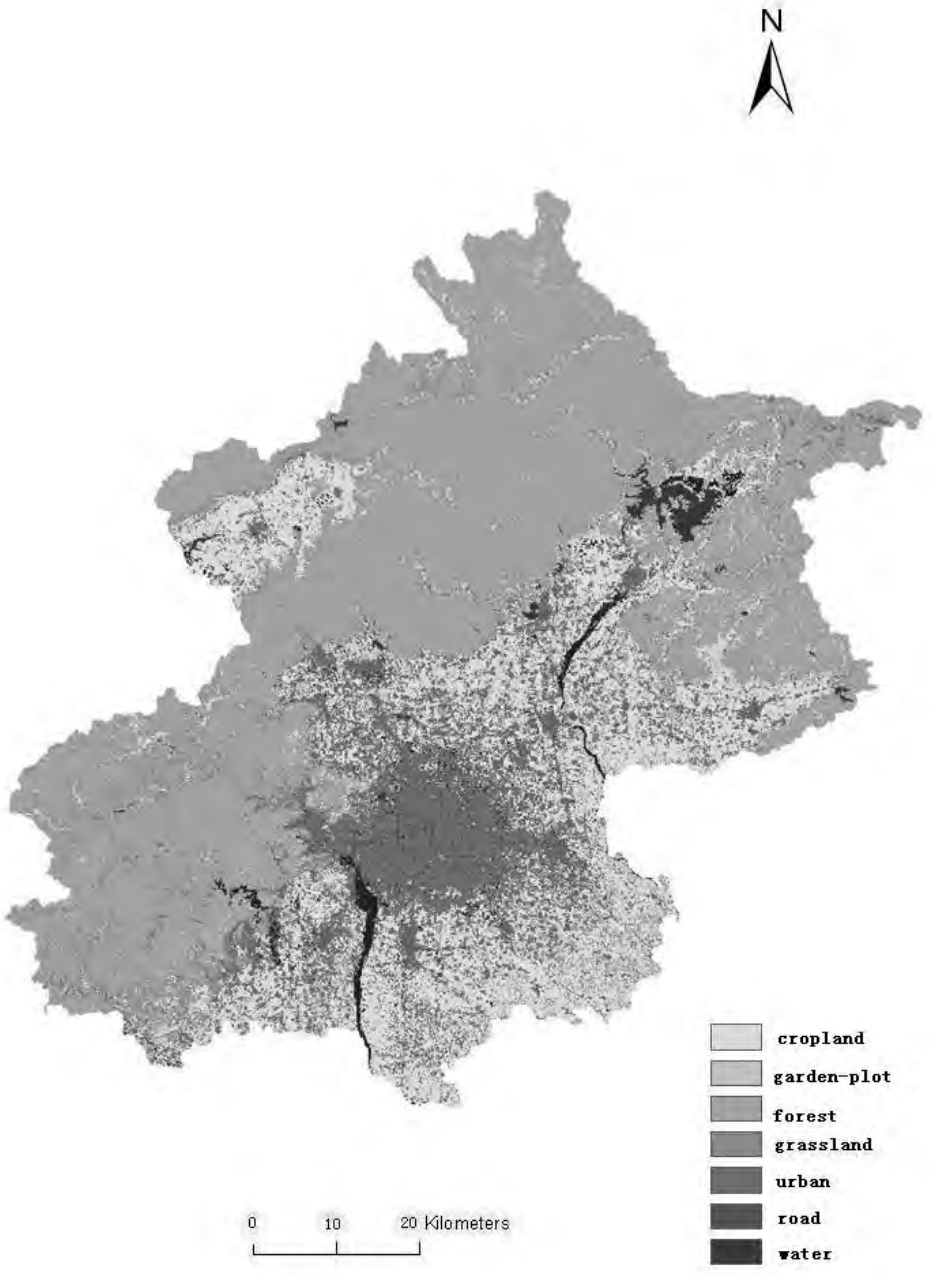

Figure 3. The map of land-use/land-cover classification at the scale of 1:100 000 in Beijing.

Validation Data

There were several intensive field observations conducted in Beijing area during 2001 to 2005, whose data can be used for validation. A summary of the experiments, including details of the instruments used, can be found in Table 1 and Table 2. Both the Shunyi and Xiaotangshan station are located in the northern suburbs of Beijing. For the Shunyi Experiment (2001), there were observation sites over maize field and over water, respectively. There was only one observation site at the Xiaotangshan Experiment 2002, but two sites (named "south" and "north" site) in 2004 and 2005. All the data were averaged every 10 minutes.

Surface temperature (T_s) was calculated by the Stefan-Boltzman law from measurements of surface radiation temperature T_r observed by an infrared radiometer and the incident longwave radiation $R_{L\downarrow}$ observed by a net radiometer, i.e., $T_s = \left(\frac{\sigma T_r^4 - (1 - \varepsilon) R_{L\downarrow}}{\varepsilon \sigma} \right)^{1/4}$. The component surface emissivity of bare soil ε_g and vegetation ε_v were measured in the field by a specific device (Xu *et al.*, 2004). The surface emissivity was then calculated from Equation 5, and their values were given in Table 3. The incident longwave radiation over water in the Shunyi Experiment was ignored because of no observations.

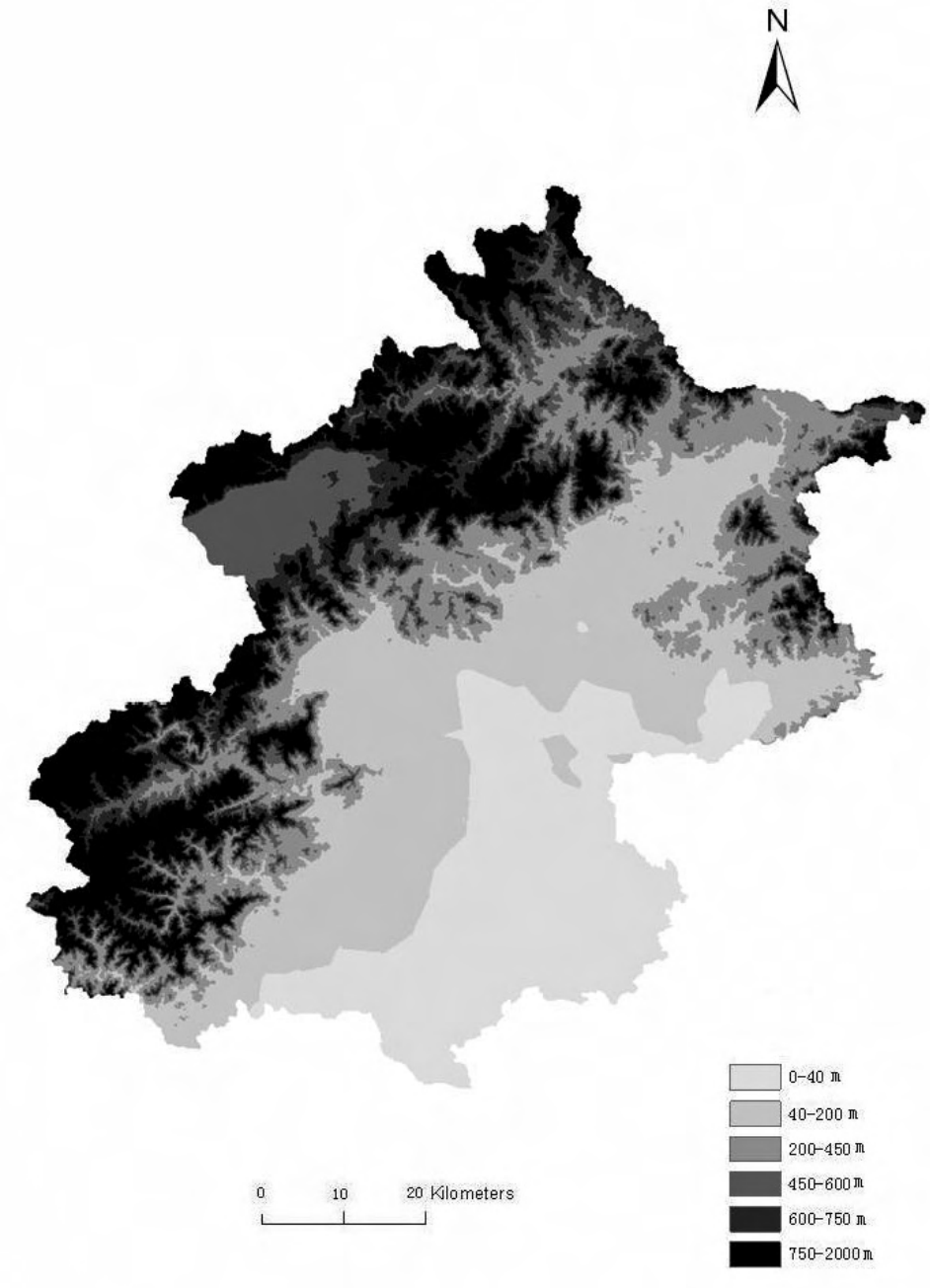

Figure 4. The DEM at the scale of 1:50 000 in Beijing.

Soil heat flux plate was placed at 2 to 3 cm below the surface. The measured values were corrected to take the soil heat storage above the plate into account; soil temperature and soil moisture data were used for this purpose (Yang *et al.*, 2004). Net radiation was measured with a net radiometer. Sensible and latent heat fluxes were measured by eddy correlation system. To avoid energy unbalance, we assume that H is accurately measured and solve for LE as a residual to the energy-balance equation (Twine *et al.*, 2000). The adjusted value was used to validate the remote sensing model. Aerodynamic resistance was calculated with the bulk transfer equation:

$$r_a = \rho C_p (T_s - T_a)/H. \quad (27)$$

Footprint

The footprint model was used to determine what area is contributing the heat fluxes (H, LE) to the sensors as well as the relative weight of each pixel inside the source area. In this study, an analytical model is used to compute the flux footprint or upwind source area contributing to the measurements of the eddy correlation system. The footprint or source weight function is expressed as (Kormann and Mixner, 2001; Guo and Cai, 2005)

TABLE 1. SITE DESCRIPTION

Observation Site	Latitude/Longitude	Surface Type	Canopy Height (m)	Duration
SY-1	40° 12′ N, 116° 34′ 1″ E	Winter Wheat Field	0.17 to 0.76	20 March to 20 May 2001
SY-2	40° 19′ N, 116° 36′ E	Water	—	01 to 17 April 2001
XTS2002	40° 10′ 1″ N, 116° 26′ 1″ E	Bare Soil	—	26 March to 08 August 2002
XTS2004-S	40° 10′ 41″ N, 116° 26′ 52″ E	Maize Field	0 to 1.5	27 May to 07 July 2004
XTS2004-N	40° 10′ 57″ N, 116° 26′ 54″ E	Grassland	0 to 0.26	27 May to 07 July 2004
XTS2005-S	40° 10′ 41″ N, 116° 26′ 53″ E	Bare Soil	—	01 May to 10 June 2005
XTS2005-N	40° 10′ 55″ N, 116° 26′ 53″ E	Grassland	0.10 to 0.39	01 May to 10 June 2005

(SY: Shunyi; XTS: Xiaotangshan; S: Southern site; N: Northern site)

TABLE 2. MEASUREMENTS TOGETHER WITH INSTRUMENTS RELEVANT TO THIS STUDY

Variables	Instruments	Instrument Height (m)	Observation Site
Sensible heat flux H Latent heat flux LE	A sonic anemometer (DA600, KAIJO, Japan) and a CO_2/H_2O analyzer (Li7500, Campbell).	2	SY-1
		2	XTS2002
	A 3D sonic anemometer (CSAT3, Campbell) and a CO_2/H_2O analyzer (Li7500, Campbell).	1.8	XTS2004-s
		1.9	XTS2004-n
		1.9	XTS2005-s
		2.0	XTS2005-n
Net radiation Rn	Net radiometer (TBB-1, China; Licor, USA)	2	SY-1
	Net radiometer (TBB-1, China)	2	XTS2002
Net radiation Rn, Incident longwave radiation flux $R_{L\downarrow}$	CNR1 net radiometer (Kipp & Zonen), Wavelength between 0.3–3, 5–50 μm.	1.5	XTS2004-s
		1.4	XTS2004-n
		1.5	XTS2005-s
		1.5	XTS2005-n
Soil heat flux G	Soil heat flux plates (HF-1, China)		SY-1
		0.02 ~ 0.03	XTS2002
	Soil heat flux plates (HFT3, USA)	below the surface	XTS2004-s
			XTS2004-n
			XTS2005-s
			XTS2005-n
Soil temperature	Soil temperature sensor (Model 107, USA)	0.0, 0.05, 0.1, 0.2, 0.4, 0.6, 0.8	XTS2004-s
		0.05, 0.1, 0.2, 0.4, 0.6, 0.8, 1.0	XTS2005-s
Soil moisture	Soil moisture meter (CS616, USA)	0.05, 0.1, 0.2, 0.4, 0.6	XTS2004-s
		0.02, 0.05, 0.2, 0.6, 1.0	XTS 2005-s
Surface radiation temperature T_s	Infrared radiometer (MX4+, Raytek, Germany, 8–14 μm)	1	SY-2
			XTS2004-s
			XTS2004-n
	Infrared Thermocouple Sensor(BS-32T, Optex, Japan, 7–20 μm)	2	XTS2002
	Infrared Thermocouple Sensor(IRT/C. sv, Campbell, 6.5–14 μm)	1.5	XTS2005-s
	Infrared Thermocouple Sensor(IRTS-P, Campbell, 6–14 μm)	1.5	XTS2005-n

TABLE 3. SURFACE EMISSIVITY AT EACH VALIDATION SITE

Date and Site (Surface)	17-04-2001 Maize Field	17-04-2001 Water	12-04-2002	06-07-2004 South	06-07-2004 North	06-05-2005 South	06-05-2005 North	22-05-2005 South	22-05-2005 North
Surface Emissivity	0.985	0.990	0.980	0.984	0.985	0.982	0.982	0.973	0.976

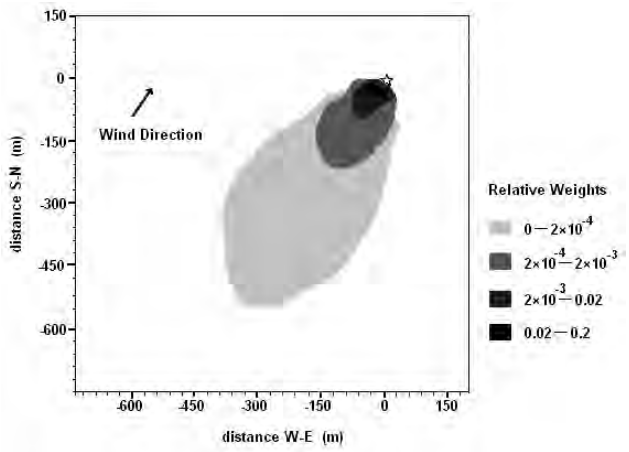

Figure 5. The flux contribution by the footprint model for XTS-N at 1040 (LT) on 06 May 2005. The star represents the eddy correlation system.

$$F = \frac{1}{\Gamma(\mu)} \frac{\xi^{\mu}}{x^{1+\mu}} e^{-\xi/x} \tag{28}$$

where F is the crosswind integrated flux footprint; Γ is the Gamma function; μ is a constant; ξ is the flux length scale; and x is the space coordinate.

An example of graphical representation of footprint on 06 May 2005 is shown in Figure 5. The result indicates that the maximum flux occurs at 30 m upwind, with 50 percent of the flux originating within 60 m of the observation site and 100 percent of the flux being within 600 m of observation site. The weights image was multiplied to the heat flux images to obtain the weighted heat flux. The weighted pixel values are then compared to the corresponding measured fluxes.

Results and Discussion

Values of surface temperature, aerodynamic resistance, net radiation, soil heat flux, sensible heat flux, and latent heat flux calculated by using TM/ETM+ data can be validated with the measurements at seven observational locations. Results are individually discussed below.

Surface Temperature

A comparison of surface temperatures between the values derived from TM/ETM+ and the measurements is shown in Figure 6a and Table 4. There is an excellent agreement between the estimates and the measurements ($R^2 = 0.938$). The remote sensing estimation is with an error about (0.53 ± 1.67)°C (MBE ± RMSE), yielding a mean absolute percent difference (MAPD) of 5.5 percent. It should be noted that the surface temperature measured is the average of point observations while the surface temperature derived from TM/ETM+ is the average at the TM/ETM+ pixel size.

Aerodynamic Resistance

A comparison of the estimated aerodynamic resistance against inverted values from measured H is presented in Figure 6b. Estimation error for r_a is 4.47 ± 18.24 sm^{-1}, yielding a MAPD of 15.9 percent for the footprint method. The result presents that the two are comparable.

Net Radiation and Soil Heat Flux

Figure 6c and 6d show the remote sensing estimate of net radiation and soil heat flux versus values measured at six observational sites. From Figure 6c it is known that the calculated Rn is very close to the field measurements, with errors of 25.16 ± 50.87 Wm^{-2} and a MAPD of 7.9 percent. This is well within the 5 percent to 10 percent error in typical net radiation measurement (Chavez *et al.*, 2005). The Landsat-based soil heat flux against the measured values is presented in Figure 6d. The remote sensing method estimates soil heat flux with an estimation error of 10.68 ± 22.81 Wm^{-2} and MAPD 19.6 percent, which do not provide a good fit to the measurements. The error may be from the difference of spatial/temporal scales between satellite data and measurements. Be note that the TM/ETM+ is in a pixel scale (30 m × 30 m), also, the estimates are instantaneous values at passing time, while the measurements are for a larger area and for average values over 10 minutes.

Sensible Heat and Latent Heat Flux

The sensible and latent heat flux (LE) calculated by the model above versus the eddy correlation measurements are shown in Figure 6e and 6f. There is a good agreement ($R^2 = 0.903$) with errors −8.56 ± 23.79 Wm^{-2} and MAPD 11.5 percent for the footprint method with adjustments for closure.

The model over-predicts LE with an error of 26.47 ± 42.54 Wm^{-2} and a MAPD of 11.9 percent ($R^2 = 0.867$) for the footprint method with adjustments for closure. This is a good result with smaller bias and a better agreement.

Spatial Distribution of Latent Heat Flux in Beijing

Figure 7 displays the spatial distribution of latent heat flux distribution (1040 local time (LT)) on 17 April 2001, 12 April 2002, 06 July 2004, 06 May 2005, and 22 May 2005, respectively in the Beijing area. LE values were quite different for different districts and counties. Reasonably, evapotranspiration was smaller in the middle area (urban) and larger in suburbs. Take 06 May 2005 as an example, LE was greater than 300 Wm^{-2} for Huairou and Pinggu districts, around 250 Wm^{-2} for Miyun, Tongzhou, Shunyi, and Daxing area, and around 200 Wm^{-2} for Yanqing, Changping, and Fangshan districts. For the urban area, such as Xicheng, Dongcheng, Xuanwu, Congwen, Chaoyang, and Fengtai, LE is below 100 Wm^{-2}.

The land-use/land-cover type in Beijing is diverse. LE for different land-use/land-cover type is quite different. As

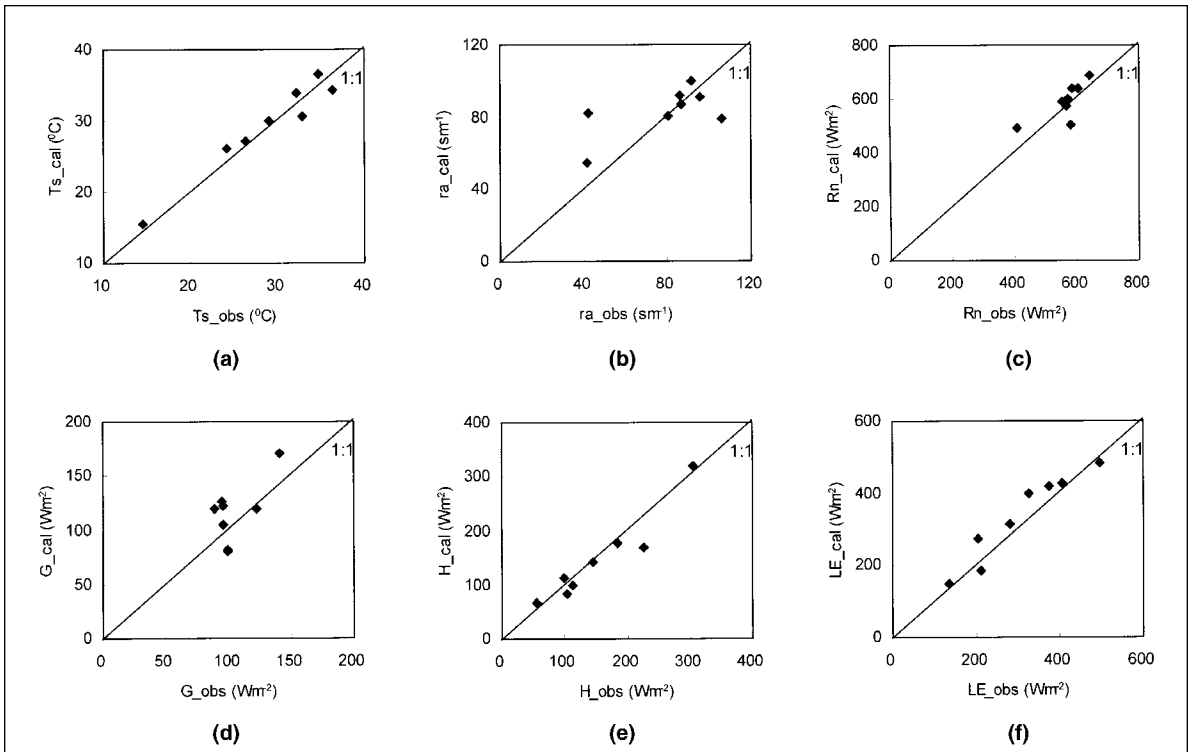

Figure 6. A comparison of the observed with the calculated values of (a) surface temperature, (b) aerodynamic resistance, (c) net radiation, (d) soil heat flux, (e) sensible heat flux, and (f) latent heat flux.

TABLE 4. OVERVIEW OF STATISTIC BETWEEN THE ESTIMATES AND THE MEASUREMENTS (T_s, R_A, RN, G, H, LE)

	T_s(°C)	r_a (sm^{-1})	Rn (Wm^{-2})	G (Wm^{-2})	H (Wm^{-2})	LE (Wm^{-2})
Sample Number	8	8	8	8	8	8
RMSD	1.67	18.24	50.87	22.81	23.79	42.54
MAPD(%)	5.5	15.9	7.9	19.6	11.5	11.9
MBE	0.53	4.47	25.16	10.68	–8.56	26.47

(RMSD: root mean square difference of retrieved value (P_i) to measured value (O_i). $RMSD = \left[1/n\sum_{i=1}^{n}(P_i - O_i)^2\right]^{1/2}$; MAPD: mean absolute percent difference of P_i to O_i, $MAPD = \frac{100}{n}\sum_{i=1}^{n}\frac{|P_i - O_i|}{\overline{O}}$; MBE: mean bias error of P_i to O_i, $MBE = \frac{1}{n}\sum_{i=1}^{n}(P_i - O_i)$)

the example above, LE for water, forest, garden-plot, cropland, grassland, road, and urban are reduced in succession. LE over water, forest and garden-plot are 451.6, 375.4, and 323.6 Wm^{-2}, respectively, while LE is only 139.5 and 8.9 Wm^{-2} over road and urban areas.

Conclusions

A new estimation model for regional ET, with TM/ETM+ data, is described in detail above which was validated with observations in 2001, 2002, 2004, and 2005, respectively. The following conclusions are drawn from this study.

Compared with ground observations, surface temperature *Ts* was well estimated by TM/ETM+ data with errors of 0.53±1.67°C. The error for net radiation estimation was 25.16±50.87 Wm^{-2}. For *G*, a larger difference existed when compared with the observations, with an error of 10.68±22.81 Wm^{-2} and a MAPD of 19.6 percent. Aerodynamic resistance r_a and sensible heat flux *H* were estimated with errors of 4.47±18.24 sm^{-1} and −8.56±23.79 Wm^{-2} for the footprint method. The latent flux LE was over-predicted with 26.47±42.54 Wm^{-2} for the footprint method with adjustments for closure. The remote sensing model proposed in this study is a feasible approach for estimating regional ET over heterogeneous surfaces.

The distribution of LE in Beijing area shows a large difference for different districts and land-use types. Evapotranspiration of water, forest, garden-plot, cropland, grassland, road and urban surfaces are reduced in succession.

To test the suitability of the model in surfaces other than Beijing area, further studies are in progress.

Acknowledgments

The authors thank the anonymous reviewers for their valuable comments and suggestions. This work was supported by the Project (40671128) funded by the NSFC, the Program for Changjiang Scholars and Innovative Research Team in University (IRT0409) and the GEF Project (TF053183).

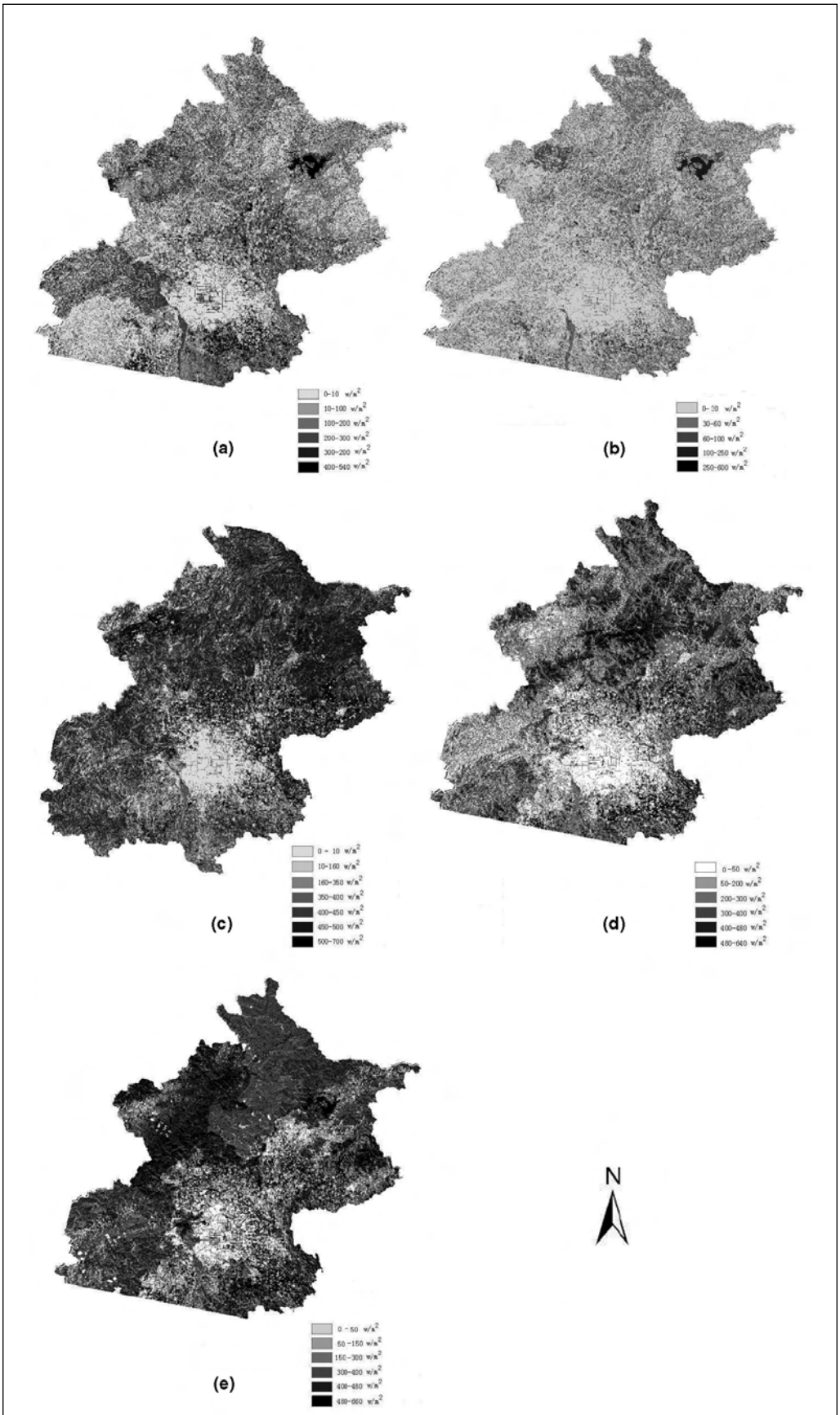

Figure 7. Spatial distribution of latent heat flux (1040 LT): (a) 17 April 2001; (b) 12 April 2002; (c) 06 July 2004; (d) 06 May 2005; and (e) 22 May 2005.

References

Bastiaanssen, W.G.M., M. Menenti, R.A. Feddes, and A.A.M. Holtslag, 1998. The surface energy balance algorithm for land (SEBAL): Part 1 Formulation, *Journal of Hydrology*, 212–213:198–212.

Bastiaanssen, W.G.M., 2000. SEBAL-based sensible and latent heat fluxes in the irrigated Gediz Basin, Turkey, *Journal of Hydrology*, 229:87–100.

Blyth, E.M., and R.J. Harding, 1995. Application of aggregation model to surface heat flux from the Sahelian tiger bush, *Agricultural and Forestry Meteorology*, 72:213–235.

Brutsaert, W., 1975. On a derivable formula for long-wave radiation from clear skies, *Water Resources Research*, 11:742–744.

Brutsaert, W., 1982. *Evaporation into the Atmosphere: Theory, History and Applications, D.* Reidel Publishing Company, Boston, 299 p.

Businger, J.A., C.J. Wyngaard, Y. Izumi, and E.F. Bradley, 1971. Flux profile relationships in the atmospheric surface layer, *Journal of the Atmospheric Sciences*, 28:181–189.

Chavez, J.L., C.M.U. Neale., L.E. Hipps, J.H. Prueger, and W.P. Kustas, 2005. Comparing aircraft-based remotely sensed energy balance fluxes with eddy covariance tower data using heat flux source area functions, *Journal of Hydrometeorology*, 6(6):923–940.

Choudhury, B.J., R.J. Reginato, and S.B. Idso, 1986. An analysis of infrared temperature observations over wheat and calculation of the latent heat flux, *Agricultural and Forest Meteorology*, 37:75–88.

Gao, Z., and L. Bian, 2002. Estimation of aerodynamic parameters in urban areas, *Quarterly Journal of Applied Meteorology*, 1:26–33 (in Chinese).

Guo, X., and X. Cai, 2005. Footprint characteristics of scalar concentration in the convective boundary layer, *Advances in Atmosphere Sciences*, 22(6):821–830.

Gutman, G., and A. Ignatov, 1998. The derivation of the green vegetation fraction from NOAA/AVHRR data for use in numerical weather prediction models, *International Journal of Remote Sensing*, 19(8):1533–1543.

Hu, J., 2005. *Study on the Temporal and Spatial Distribution of Surface UHI (Urban Heat Island) in Beijing Urban Area and Analysis of its Main Relative Factors*, Ph. D. Dissertation, Beijing Normal University, Beijing, China, 147 p. (in Chinese).

Jackson, R.D., S.B. Idso, R.J. Reginato, P.J. Pinter, 1981. Canopy temperature as a crop water stress indicator, *Water Resources Research*, 17(4):1133–1138.

Jackson, R.D., 1985. Evaluating evapotranspiration at local and regional scales, *Proceedings of IEEE*, 73:1086–1096.

Kormann, R., and F.X. Meixner, 2001. An analytical footprint model for non-neutral stratification, *Boundary-Layer Meteorology*, 99:207–224.

Kustas, W.P., B.J. Choudhury, M.S. Moran, R.J. Reginato, R.D. Jackson, L.W. Gay, and H.L. Weaver, 1989. Determination of sensible heat flux over sparse canopy using thermal infrared data, *Agricultural and Forest Meteorology*, 44:197–216.

Liang, S., 2001. Narrowband to broadband conversions of land surface albedo: Algorithms, *Remote Sensing of Environment*, 76:213–238.

Menenti, M., and B.J. Choudhury, 1993. Parameterization of land surface evapotranspiration using a location-dependent potential evapotranspiration ans surface temperature range, *Exchange Process at the Land Surface for a Range of Space and Time Scales* (H.J. Bolle, R.A. Feddes, and J.D. Kalma, editors), International Association of Hydrological Sciences, Publication No. 212, pp. 561–568.

Moran, M.S., T.R. Clarke, Y. Inoue, and A. Vidal, 1994. Estimating crop water deficit using the relation between surface air temperature and spectral vegetation index, *Remote Sensing of Environment*, 49:246–263.

Moran, M.S., A.F. Rahman, J.C. Washburne, D.C. Goodrich, M.A. Weltz, and W.P. Kustas, 1996. Combining the Penman-Monteith equation with measurements of surface temperature and reflectance to estimate evaporation rates of semiarid grassland, *Agricultural and Forest Meteorology*, 80:87–109.

Norman, J.M., W.P. Kustas, and K.S. Humes, 1995. Source approach for estimating soil and vegetation energy fluxes in observations of directional radiometric surface temperature, *Agricultural and Forest Meteorology*, 77:263–293.

Paulson, C.A., 1970. The mathematical representation of wind speed and temperature profiles in the unstable atmospheric surface layer, *Journal of Applied Meteorology*, 9:857–861.

Qin Z., M. Zhang, A. Karnieli, and P. Berliner, 2001. Mono-window algorithm for retrieving land surface temperature from Landsat TM6 data, *Acta Geographica Sinica*, 4(56):456–466 (in Chinese).

Shuttleworth, W.J., and J.S. Wallace, 1985. Evaporation from sparse crops: An energy combination theory, *Quarterly Journal of the Royal Meteorological Society*, 111(469):839–855.

Sobrino, J.A., J.C. Jimenez-Munoz, and L. Paolini, 2004. Land surface temperature retrieval from Landsat TM5, *Remote Sensing of Environment*, 90:434–440.

Soushi, K., 2005. Analysis of urban heat-island effect using ASTER and ETM+ data: Separation of anthropogenic heat discharge and natural heat radiation from sensible heat flux, *Remote Sensing of Environment*, 99:44–54.

Su, Z., 2002. The surface energy balance system (SEBS) for estimation of turbulent heat fluxes, *Hydrology & Earth System Sciences*, 6(1):85–99.

Tu, Q.P., D.M. Weng, Q. Wu, Y.Q. Jiang, and L.N. Pan, 1978. Study on the correction method of short-term climatic data (I), *Journal of Nanjing Institute of Meteorology*, 1:59–67 (in Chinese).

Twine, T.E., W.P. Kustas, J.M. Norman, D.R. Cook, P.R. Houser, T.P. Meyers, J.H. Prueger, P.J. Starks, and M.L Wesly, 2000. Correcting eddy-covariance flux underestimates over a grassland, *Agricultural and Forest Meteorology*, 103:279–300.

Valor, E., and V. Caselles, 1996. Mapping land surface emissivity from NDVI: Application to European, African and South American areas, *Remote Sensing of Environment*, 57:167–184

Waters, R., R. Allen, M. Tasumi, R. Trezza, and W. Bastiaanssen, 2002. *SEBAL (Surface Energy Balance Algorithms for Land): Advanced Training and Users Manual*, Version 1.0, University of Idaho, 98 p.

Webb, E.K., 1970. Profile relationships: The log-linear range and extension to strong stability, *Quarterly Journal of the Royal Meteorological Society*, 96:67–90.

Weng, D., and Z. Sun, 1984. A preliminary study of the lapse rate of surface air temperature over mountainous regions of China, *Geographical Research*, 3(2):24–34 (in Chinese).

Xu, J., X. Sun, and R. Zhang, 2004. Measuring of thermal radiation multi-reflection information in soil-vegetation system, *Proceedings of IEEE 2004 International Geoscience and Remote Sensing Symposium*, 20–24 September, Anchorage, Alaska, unpaginated CD-ROM.

Yang, K., T. Koike, H. Ishikawa, and Y. Mao, 2004. Analysis of the surface energy budget at a site of GAME/Tibet using a single-source model, *Journal of the Meteorological Society of Japan*, 82(1):131–153.

Zhang, R., X. Sun, J. Liu, H. Su, X. Tang, and Z. Zhu, 2003. Determination of regional distribution of crop transpiration and soil water use efficiency using quantitative remote sensing data through inversion, *Science in China (Series D)*, 46(1):10–22.